Food Chemistry: X 27 (2025) 102446

Contents lists available at ScienceDirect

Food Chemistry: X

journal homepage: www.sciencedirect.com/journal/food-chemistry-x

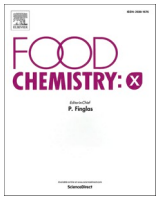

Volatile profiling from thermal decomposition of Amadori compounds in the alanine-glucose Maillard reaction: An DFT insight of 3-ethyl-2,5-dimethylpyrazine forming mechanism

Pengxun Gao [a,b,1], Shang Wang [c,1], Baomin Feng [a], Chunying Liu [a], Yi Wang [c], Shaohua Dou [a,*], Liang Dong [a,**]

[a] College of Life and Health, Dalian Key Laboratory of Animal Immunization, Liaoning Marine Microorganism Engineering and Technology Research Center, Dalian University, Dalian 116622, Liaoning, China
[b] School of Food Science and Technology, National Engineering Research Center of Seafood, Dalian Polytechnic University, Dalian 116034, Liaoning, China
[c] School of Biotechnology, Dalian Polytechnic University, Dalian 116034, Liaoning, China

ARTICLE INFO

Keywords:
Amadori rearrangement products
Maillard reaction
3-ethyl-2,5-dimethylpyrazine
Volatile compounds
GC–MS

ABSTRACT

The composition of volatile compounds generated by the thermal decomposition of Amadori rearrangement products (ARPs) in the Maillard reaction between glucose and alanine was investigated by using a combination of thermal desorption cryo-trapping system and gas chromatography–mass spectrometry. A total of 25 volatile compounds were detected and identified, including 15 pyrazines, 3 pyridines, 1 pyrrole, and 6 complex nitrogen-containing compounds. The results indicated that pyrazines are the predominant products of the thermal decomposition of ARPs, and the specific formation temperatures of the various volatiles were determined. Additionally, density functional theory (DFT) was employed to study the formation mechanism of 3-ethyl-2,5-dimethylpyrazine in depth, and the structures of the reactants, transition states, and products were elucidated. Furthermore, by comparing the rate constants and reaction energy barriers of the different reactions, it was concluded that the synthesis of deoxyglucosones and the ring-forming reaction of pyrazines are the key reactions in the generation pathway of 3-ethyl-2,5-dimethylpyrazine.

1. Introduction

The Maillard reaction is a non-enzymatic browning phenomenon that occurs during food processing, involving the reaction between carbonyl compounds (reducing sugars) and amino compounds (Cui et al., 2021; Lu et al., 2014). This reaction can be delineated into three distinct stages (Nagai et al., 2014). Initially, condensation between amino-containing compounds and carbonyl-containing compounds leads to the formation of Schiff bases, which then cyclize to produce N-glucosylamines. These intermediates undergo Amadori rearrangement to generate dicarbonyl compounds. (Won & Lee, 2001). Subsequently, the rearrangement triggers the degradation of deoxyglucosone, involving the strecker reaction of the amino acid with the dicarbonyl compound. (Guerra & Yaylayan, 2012). The final stage involves condensation and polymerization of hydroxyaldehyde to form the characteristic brown pigment. Notably, the Amadori rearrangement reaction is considered the pivotal step in the entire Maillard reaction (Jalbout et al., 2007).

Meanwhile, ARPs have been identified as stable intermediates of the Maillard reaction, capable of undergoing further thermal decomposition to yield a plethora of aroma substances (Yu et al., 2019). Consequently, ARPs are regarded as potential food flavor enhancers, often incorporated into food during thermal processing to augment the Maillard reaction and subsequent aroma development (Gaudette & Pietrasik, 2017). Among the thermal decomposition products of ARPs, pyrazines are particularly abundant. Notably, 3-ethyl-2,5-dimethylpyrazine stands out as a flavor-active compound characterized by a roasted, nutty aroma, and is considered as a key aroma compound in thermally

* Corresponding author.
** Corresponding authors at: College of Life and Health, Dalian University, Dalian Economic and Technological Development Zone, Xuefu Street No. 10, Dalian 116622, Liaoning, China.
E-mail addresses: doushaohua@dlu.edu.cn (S. Dou), dongliang@dlu.edu.cn (L. Dong).
[1] Pengxun Gao and Shang Wang contributed equally to this study

https://doi.org/10.1016/j.fochx.2025.102446
Received 4 January 2025; Received in revised form 4 April 2025; Accepted 5 April 2025
Available online 6 April 2025
2590-1575/© 2025 The Authors. Published by Elsevier Ltd. This is an open access article under the CC BY-NC-ND license (http://creativecommons.org/licenses/by-nc-nd/4.0/).

processed foods such as coffee, chocolate, and roasted meats (Motoyama et al., 2021). Its remarkable stability under heat and low odor threshold renders it invaluable for flavor enhancement, surpassing less stable or more ubiquitous volatiles like simple aldehydes or furans. Moreover, the alkyl-substituted pyrazine core of 3-ethyl-2,5-dimethylpyrazine provides a judicious balance of stability and reactivity, rendering it an ideal candidate for mechanistic studies (Cho & Kays, 2013; Mortzfeld et al., 2020). Consequently, investigating the formation mechanism of 3-ethyl-2,5-dimethylpyrazine holds profound theoretical significance for comprehending the genesis of pyrazines within the Maillard reaction and elucidating the intricate mechanisms governing the Maillard reaction itself.

Density functional theory (DFT), a cornerstone in theoretical chemistry, has gained widespread application across various fields in recent years (Parr, 1980; Wang et al., 2023). It empowers the calculation of molecular structures, reaction parameters, transition states, and products during chemical reactions. Additionally, DFT facilitates the identification of active sites within functional groups and the determination of reaction activation energies (Quapp, 2010). The integration of DFT into the study of the Maillard reaction offers a powerful tool for elucidating the formation mechanisms of aroma substances (Orhan et al., 2005; Takken et al., 1975). In this study, we initially analyzed the composition of thermal decomposition volatiles generated by ARPs in the glucose-alanine Maillard reaction. We determined the generation temperatures of various volatiles and elucidated the influence of temperature on their formation. Subsequently, DFT was employed to investigate the generation mechanism of 3-ethyl-2,5-dimethylpyrazine, the most abundant thermal decomposition product, thereby providing a theoretical foundation for revealing the flavor formation mechanism of the Maillard reaction.

2. Experimental

2.1. Chemicals

D-glucose (99.5 %), L-alanine (99 %), o-dichlorobenzene (99 %), $NaHSO_3$ (AR), and ethanol (95 %, AR) were purchased from Macklin (Shanghai, China). Glycerol and acetic acid were purchased from Damao Chemical Reagent Co. Dowex 50WX4 ion exchange resin-H^+ type was purchased from Aladdin (Shanghai, China). Ultrapure water (UPW) was used for all experiments.

2.2. Preparation and purification of ARPs in the alanine-glucose Maillard reaction

ARPs of glucose-alanine Maillard reaction was prepared by following the method of Glinsky et al. with certain modifications (Glinsky et al., 1996). 0.2 mol of D-(+) glucose, 2.0 g of sodium bisulfite, 60 mL of anhydrous ethanol, and 30 mL of glycerol were added to a round-bottomed flask, and were heated in a water bath and subjected to condensation reflux. When the solution reaches 100 °C, 0.05 mol of L-alanine and 8 mL of acetic acid were added. The mixed solution was heated at 80 °C for 5 h and then cooled to room temperature with ice water. Then, samples were taken by loading activated H^+ Dowex 50WX4 ion exchange resin onto a 40 mm × 400 mm column. The column was eluted with water (2 mL/min) and stopped when the eluate was negative for TTC, and then eluted with 1 mol/L ammonia (1 mL/min). The eluate was concentrated on a rotary evaporator and then freeze-dried to a solid powder.

2.3. Extraction and collection of volatile compounds from ARPs during heating by using a thermal desorption cryo-trapping system

Simulative heating was conducted using a certified micro-chamber/thermal extractor (M-CTE, M-CTE250, Markes International, UK). The M-CTE250 serves as a quality control instrument for the screening of volatile and semi-volatile organic compounds emitted from organic materials. Prior to use, the M-CTE was decontaminated to eliminate any residual pollutants. The chambers, o-rings, and sample holders of the M-CTE were initially rinsed with ethanol and cyclohexane. Subsequently, a 20-mL glass vial was positioned in the sample holder, and 0.01 g of ARPs along with 10 μL of diluted ortho-dichlorobenzene (0.5 mg/L) as the quantitative internal standard were directly introduced into the vial. The sample holder's lid was then promptly sealed. Three sample holders were employed concurrently for parallel experiments (one sample per chamber) and were heated at 60, 80, 100, 120, 140, 150, 160, 170, and 180 °C for 30 min each. Following the heating period, the air valve was opened at a flow rate of 100 mL/min for 30 min per temperature setting to extract volatiles from the samples. These compounds were captured in 250 mg Tenax TA adsorbent tubes (60–80 mesh). After trapping, the volatile compounds were thermally desorbed from the sorbent tubes using an automated thermal desorber (TD100-xr, Markes International) at 280 °C for 5 min, cryo-focused on a cold trap at 10 °C, and desorbed from the cold trap onto the GC–MS column by flash heating at 280 °C for 3 min, with a flow path temperature of 200 °C.

2.4. GC–MS analysis

An Agilent 6890/5975C GC–MS system (Santa Clara, CA, USA), furnished with an HP-5 ms column (30 m × 0.25 mm i.d., 0.25 μm film thickness; J&W Scientific), was employed for the analysis of volatiles desorbed from the cold trap. Helium was utilized as the carrier gas in splitless mode, with a flow rate of 1 mL/min. The desorption duration in the injection port was set at 5 min at 250 °C. The temperature program entailed an initial hold at 35 °C for 3 min, followed by a ramp to 280 °C at a rate of 5 °C/min. The mass selective detector functioned in electron impact ionization mode at 70 eV, scanning the mass range 40–400 *m/z*. The interface temperature was set at 230 °C. The retention times of the volatiles were converted to Kovats retention indices using n-alkanes (Sigma, Co.) as standards. Tentative identification of the volatile compounds was achieved by comparing their mass spectra with those of reference compounds in both the Wiley MS library (8th edn) and the NIST/EPA/NIH MS library (2014 version). Confirmation was based on literature mass spectra and comparison of calculated Kovats retention indices with published data. The accuracy of identification was ascertained by analyzing relevant standard compounds via GC–MS under identical operational conditions.

2.5. MALDI-ToF/ToF mass spectrometry

The DHB matrix was prepared at 15 mg/mL in 50 % methanol (aqueous) and 0.1 % trifluoroacetic acid. 3–5 mg of glucose-alanine ARPs was dissolved in 1 mL of ultrapure water. After centrifugation at 10,000 rpm for 5 min, 1 μL of the supernatant is mixed with 1 μL of the matrix. Then, 1 μL of the mixture was deposited onto a ground stainless steel 384-density MALDI plate and allowed air dry naturally. The AutoflexTM Speed ToF/ToF mass spectrometer (Bruker Daltonics, Berlin, DE) was used in positive ion mode with the following specific parameters: voltage of 4500 V; Nebulizer at 0.3 Bar; Dry Gas at 4.0 L/min, with a drying temperature of 200 °C; laser: nitrogen laser with a wavelength of 335 nm; relative laser intensity of 90 % as used; frequency of 1000 Hz; Ion source 1 at 19.62 kV; Ion source 2 at 18.29 kV; Lens at 7 kV; Pulsed Ion Extraction of 350 ms; linear 10×.

2.6. Computational methods

All computations in this study were performed using the Gaussian16 software package. Geometry optimizations for molecular ions, intermediates, and fragments were conducted at the UB3LYP density functional theory level with the 6-311G (d,p) basis set. This basis set was widely employed for structural optimization and transition state calculations due to its balance of accuracy and computational efficiency.

Transition state (TS) geometries were located at the same theoretical level, and the resulting TSs were confirmed to possess a single imaginary frequency, indicative of a true TS. All identified TS geometries were validated by calculating the intrinsic reaction coordinate (IRC). Point singlet state energies were computed using the high-level Def2TZVP basis set, and these data were combined with frequency calculation results using the Gibbs free energy plugin, Shermo 2.0.8, to construct precise reaction potential energy surfaces. The energy value closest to the reaction saddle point was identified as the Gibbs free energy required for the reaction to proceed. Reaction rate constants were determined from the characterized potential energy surfaces, the properties of the reactants, and the TSs. The activation free energy (ΔG*) was estimated from the relative energies, including zero-point energy (ZPE) corrections, between the TSs and reactants. The TST calculator was utilized to calculate the reaction rate constants. The Multiwfn package was employed to compute the approximation functions for molecular structures.

2.7. Statistical analysis

All experiments were conducted in triplicate. The measured data were analyzed using PCA by the MetaboAnalyst 3.0. Significance between related samples was analyzed according to the one-way ANOVA test at the level of 0.05 ($p < 0.05$) using the SPSS 18.0 (Chicago, IL, USA).

3. Results and discussion

3.1. Analysis of ARPs based on MALDI-ToF/ToF mass spectrometry

The structure of ARPs in the alanine-glucose Maillard reaction is shown in Fig. 1 (A). As depicted in Fig. 1 (B), the molecular weight of this compound is 251 Da. Moreover, its imino group readily associates with protons in the positive ion mode, forming a parent ion with m/z = 252 ($[M + H]^+$). This corresponds to the fragment peaks at m/z = 251.0012 and m/z = 252.0055 in the spectrum. Therefore, this substance can be confirmed as the ARPs of the glucose-alanine Maillard reaction.

3.2. Composition of volatile compounds from ARPs decomposition during heating

As shown in Table 1, based on the chromatographic peak mass spectra and the standard spectra of NIST standard mass spectral library as well as the comprehensive comparison of standard compounds, a total of 25 volatile compounds were identified, including pyridine (3), pyrrole (1), pyrazine (15), and complex N-containing compounds (6). The total ion flow diagram of the volatiles is shown in Fig. 2. As can be seen from Table 1, pyrazines are relatively large in both quantity and relative abundance among all volatile compounds, which suggests that pyrazines are the main products of the ARPs thermal decomposition. It was also found that among these pyrazines the main ones were alkyl pyrazines, including 11 species, and all of them had simple alkyl side chains. In addition, there were two pyrazines with alkenyl side chains and one pyrazine with an acetyl group. The generation of alkenyl as well as acyl groups is considered to be the product of Strecker reaction (Ma et al., 2022). Pyrazines are usually colorless with some weak basicity and are isomers with pyrimidines and pyridazines (Long et al., 1973). Pyrazines do not readily undergo electrophilic substitution but react readily with nucleophilic reagents (Brittain et al., 1979). They are commonly used as pharmaceutical, flavors and fragrances intermediates (Higashio & Shoji, 2004). Besides, among the thermal decomposition products of ARPs, pyrroles are another N-containing substance that are usually colorless or slightly yellowish liquids with a nutty and fruity flavor (Mizuguchi, 2005). And pyridines, a series of six-membered heterocyclic compounds, are used as an industrial denaturant and dyeing aid (Portella et al., 2015).

3.3. Impact of temperature on volatile compounds forming from ARPs decomposition during heating

The food heating process is usually very complex, with many chemical reactions occur. In order to explore the thermal decomposition process of ARPs, a thermal desorption cryo-trapping system was used to simulate the heating process in this study, and nine temperature points (60 °C, 80 °C, 100 °C, 120 °C, 140 °C, 150 °C, 160 °C, 170 °C, and 180 °C) were chosen to evaluate the effect of temperature on the volatile compounds formed from ARPs thermal decomposition. Results show that 2, 1, 2, 3, 11, 1, 2, and 3 newly generated volatiles were identified at different temperature points, respectively. Fig. 3 visualized the formation temperatures of the different volatiles from ARPs during heating, as well as the composition of the volatiles in each temperature point.

As shown in Fig. 3(A), two substances were detected to be produced at 60 °C (2,4,6-trimethylpyridine, 2,5-dimethylpyrazine). Compared to the reported literature, the formation temperature of 2,5-dimethylpyrazine is significantly lower, and its contents is higher (Lu et al., 2005; van Lancker et al., 2010). As the temperature increased to 80 °C, one newly produced substance was detected (3-ethyl-2,5-dimethylpyrazine). This compound is colorless with the aroma of peanuts, nuts, and coffee (Evershed et al., 1982). It also has the lower forming temperature and higher content compared to the literature reported (Cai et al., 2016; Lu et al., 2005). Two newly formed substances (2-ethyl-5-methylpyrazine,

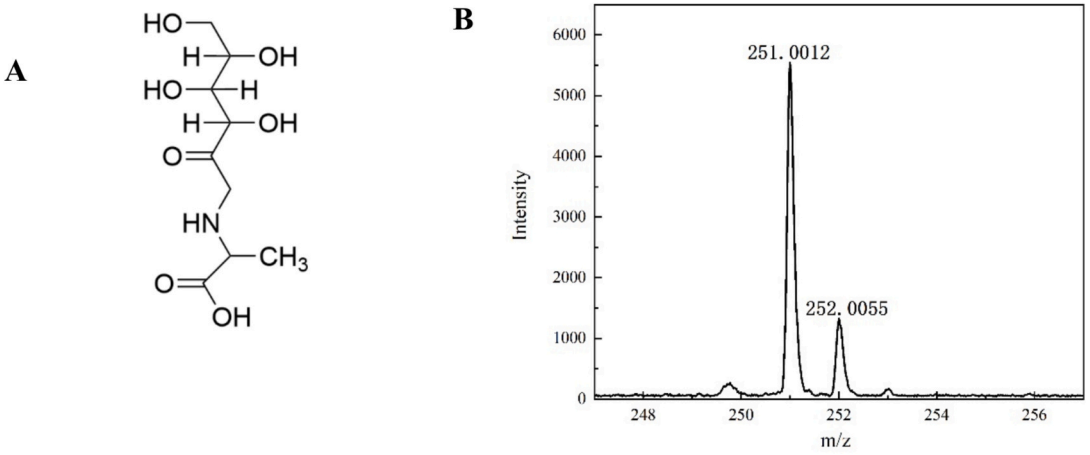

Fig. 1. Alanine - Glucose - ARPs structure information. A: Structure; B: MALDI-ToF/ToF mass spectrum of ARPs.

Table 1
Volatile compounds generated in Alanine - Glucose - ARPs thermal decomposition process.

No.	compound	RI	Identification method	Concentration(ug/g)								
				60 °C	80 °C	100 °C	120 °C	140 °C	150 °C	160 °C	170 °C	180 °C
1	N-ethylpyridine	821	RI,MS	nd	nd	nd	nd	nd	nd	49.68 ± 13.25b	69.15 ± 1.19a	57.89 ± 12.82b
2	2,4,6- trimethylpyridine	991	RI,MS,STD	7.94 ± 1.86a	5.74 ± 1.03a	8.12 ± 1.18a	1.92 ± 1.78b	nd	nd	nd	nd	nd
3	3-methyl-5-ethylpyridine	1023	RI,MS,STD	nd	nd	nd	nd	nd	nd	nd	21.70 ± 1.18a	23.58 ± 4.12a
4	2-ethylpyrrole	850	RI,MS,STD	nd	nd	nd	nd	40.85 ± 20.48a	nd	nd	nd	nd
5	2,5-dimethyl pyrazine	917	RI,MS,STD	2.78 ± 1.18f	8.98 ± 2.02e	27.68 ± 19.43d	57.96 ± 31.62c	229.24 ± 23.62a	63.40 ± 30.62c	209.63 ± 26.37a	197.91 ± 8.47a	171.60 ± 33.72b
6	2-ethyl-5-methylpyrazine	1005	RI,MS,STD	nd	nd	18.63 ± 15.12d	47.89 ± 11.13c	295.08 ± 58.47a	76.09 ± 23.55c	209.27 ± 48.13b	222.78 ± 9.70b	195.75 ± 32.43b
7	3-ethyl-2,5-dimethylpyrazine	1082	RI,MS,STD	nd	11.04 ± 8.16e	62.46 ± 52.72d	189.68 ± 33.39d	1243.25 ± 378.62a	495.40 ± 21.07c	1010.61 ± 142.90a	860.32 ± 99.22b	788.14 ± 162.36b
8	2-methyl-5-(2-propenyl)-pyrazine	1090	RI,MS,STD	nd	nd	nd	nd	29.37 ± 23.04a	19.28 ± 1.55a	30.53 ± 5.51a	19.93 ± 7.52a	27.47 ± 2.46a
9	3,5-diethyl-2-methylpyrazine	1162	RI,MS,STD	nd	nd	9.36 ± 8.13d	28.68 ± 15.83d	674.58 ± 262.91a	119.65 ± 35.61c	367.45 ± 139.91b	384.98 ± 36.94b	291.83 ± 129.15b
10	2,3,5-trimethyl-6-ethylpyrazine	1163	RI,MS,STD	nd	nd	nd	nd	249.27 ± 91.04a	112.93 ± 12.06b	263.41 ± 96.77a	223.17 ± 0.69a	198.02 ± 27.00a
11	2-acetyl-3-ethylpyrazine	1168	RI,MS,STD	nd	nd	nd	nd	73.25 ± 26.66a	21.28 ± 2.01c	49.73 ± 17.78b	48.16 ± 0.27b	48.35 ± 6.58b
12	2,3-dimethyl-5-n-propylpyrazine	1166	RI,MS,STD	nd	nd	nd	nd	33.23 ± 17.41a	nd	nd	7.74 ± 1.32b	8.74 ± 0.84b
13	2,5-dimethyl-3-(1-methylpropyl)-pyrazine	1194	RI,MS	nd	nd	nd	nd	83.81 ± 35.95a	nd	16.54 ± 6.10b	14.87 ± 1.87b	18.00 ± 2.64b
14	2,3-dimethyl-5-(1-methylpropyl)-pyrazine	1187	RI,MS,STD	nd	nd	nd	nd	nd	10.48 ± 4.24b	36.60 ± 17.35a	41.81 ± 2.58a	44.42 ± 7.34a
15	2,3,5-trimethyl-6-propylpyrazine	1257	RI,MS,STD	nd	nd	nd	1.67 ± 0.66d	89.93 ± 40.52a	14.33 ± 5.78c	43.41 ± 19.88b	45.30 ± 2.26b	48.97 ± 7.19b
16	2-butyl-3,5-dimethylpyrazine	1254	RI,MS,STD	nd	nd	nd	nd	37.03 ± 6.93a	9.20 ± 2.05c	22.92 ± 10.76b	23.75 ± 0.93b	16.31 ± 7.24b
17	2,3,5-trimethyl-1-propenyl-(*Z*)-pyrazine	1434	RI,MS	nd	nd	nd	nd	52.72 ± 42.70a	24.16 ± 7.46b	50.79 ± 26.56a	54.11 ± 2.76a	68.11 ± 11.39a
18	3,6-dipropyl-2,5-dimethylpyrazine	1663	RI,MS,STD	nd	nd	nd	nd	41.40 ± 24.12a	5.42 ± 1.96c	18.34 ± 10.60b	21.14 ± 2.11b	30.26 ± 7.31a
19	6,7-dihydro-2,5-dimethyl-5H-cyclopentapyrazine	1225	RI,MS	nd	nd	nd	nd	nd	nd	nd	16.46 ± 1.33b	21.73 ± 3.17a
20	2-(1-oxobut-2-ynyl)-cyclohexanone	1663	RI,MS	nd	nd	nd	6.17 ± 4.23d	288.54 ± 89.13a	35.82 ± 13.20c	90.06 ± 39.37b	91.09 ± 8.30b	90.37 ± 11.98b
21	2,3,5,6-tetramethyl-1,4-phenylenediamine	1430	RI,MS	nd	nd	nd	8.92 ± 5.81d	500.88 ± 206.68a	35.86 ± 17.73c	193.57 ± 97.55b	227.26 ± 21.79b	217.29 ± 32.99b
22	N4,N4-diethyl-2-methyl-1,4-benzenediamine	1636	RI,MS	nd	nd	nd	nd	141.36 ± 72.95a	25.87 ± 11.66c	66.62 ± 30.82b	71.38 ± 97.47b	74.56 ± 32.99b
23	3-(pyrrolidine-1-yl)-aniline	1566	RI,MS	nd	nd	nd	nd	nd	nd	nd	25.24 ± 1.79b	35.26 ± 5.60a
24	5,6-dimethyl-2-benzimidazolinone	1267	RI,MS	nd	nd	nd	nd	nd	nd	28.40 ± 14.91b	28.89 ± 1.94b	38.34 ± 5.99a
25	8-aminoquinaldine	1488	RI,MS	nd	nd	nd	nd	34.39 ± 16.67c	48.37 ± 27.91b	71.73 ± 30.45a	59.55 ± 7.56a	79.49 ± 5.14a

Nd = Compound not detected in the sample. MS = Identification by MS spectra, RI = Kovat's retention indexes, STD = Comparison with a standard compound; Concentration is the mean ± standard error of three replicates; "a,b, c, d" indicates a significant difference ($p < 0.05$).

3,5-diethyl-2-methylpyrazine) were detected at 100 °C. 2-ethyl-5-methylpyrazine was reported to be generated at 130–140 °C (van Lancker et al., 2012; Yu et al., 2013). 3,5-diethyl-2-methylpyrazine is usually used in bakery products (Tan & Yu, 2012). It can be seen that when the temperature was lower than 100 °C, the products were only alkyl pyrazines with a relatively simple side chain structure. When the temperature increased to 120 °C, three substances were formed, including 2,3,5-trimethyl-6-propylpyrazine, 2-(1-oxobut-2-ynyl)-cyclohexanone, 2,3,5,6-tetramethyl-1,4-phenylenediamine.

As the temperature continue to increase, a total of 11 new substances were detected at 140 °C, including 2,3,5-trimethyl-6-ethylpyrazine, 2-acetyl-3-ethylpyrazine, 2,3-dimethyl-5-n-propylpyrazine, 2,5-dimethyl-3-(1-methylpropyl)-pyrazine, 2-butyl-3,5- dimethylpyrazine, 2,3,5-trimethyl-1-propenyl-(*Z*)-pyrazine, 3,6-dipropyl-2,5-dimethylpyrazine, 2-ethylpyrrole, 2-methyl-5-(2-propenyl)-pyridine, N4,N4-diethyl-2-methyl-1,4-benzenediamine and 8-aminoquinaldine. It is clearly that in this temperature point the relative content of most volatiles have a significant increase to reach at their highest, and their structures also show a tendency to become more complex in their side chains such as pyrazines (Gómez-Míguez et al., 2007). Therefore, 140 °C was considered to be a crucial temperature point for the pyrazine formation. Only one (2,3-dimethyl-5-(1-methylpropyl)-pyrazine) and two (N-ethylpyridine, 5,6-dimethyl-2-benzimidazolinone) new substances were generated at temperatures of 150 °C and 160 °C, respectively. When the

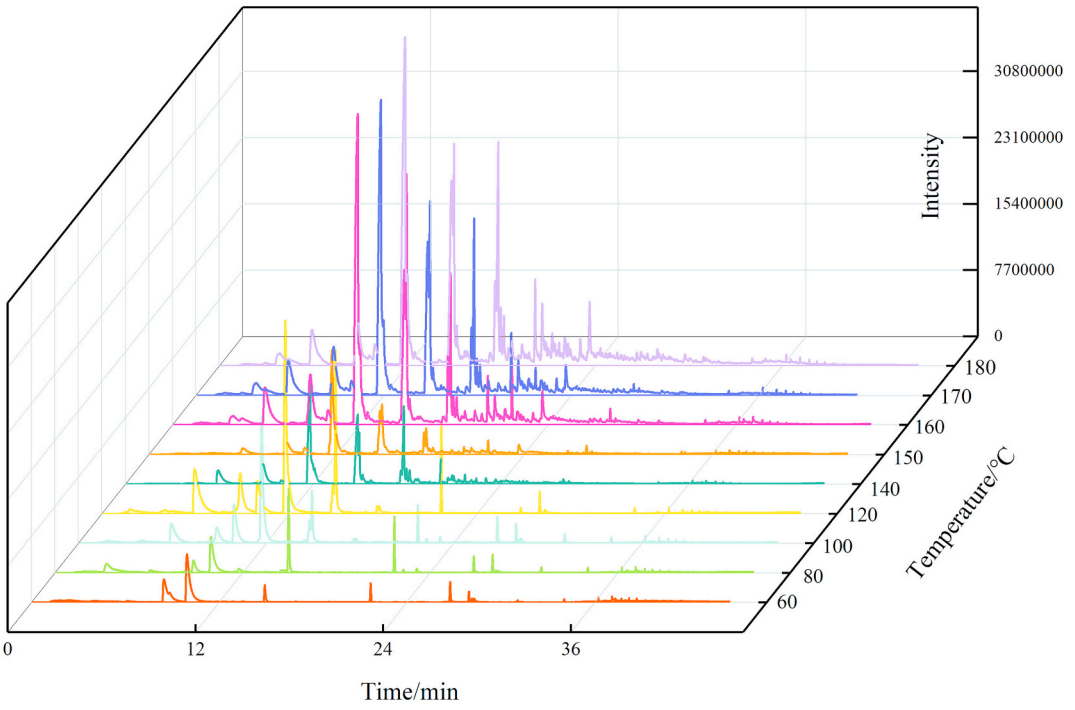

Fig. 2. Total ion current chromatograms of Alanine - Glucose - ARPs thermal decomposition based on GC–MS.

temperature was higher than 170 °C, there was no new pyrazines formed, and nearly all volatiles could be detected in the highest amount (Fig. 3(B)). Meanwhile, a heat map was drawn to assess the trends of each volatile compound at different temperatures. As shown in Fig. 3(B), the colors of the heat map show a graduation from cool to warm. Cooler colors represent lower content and warmer colors represent relatively higher content. As the temperature increases, the color of most volatile compounds gradually warms from cold, which indicates that the content of most volatiles increases with increasing temperature.

In order to better understand the composition of ARPs thermal decomposition and changing characteristics during heating, a principal component analysis (PCA) was applied, and the scoring scatter and loading scatter plots are shown in Figs. 4(A) and 4(B), respectively. The first two major components, PC1 and PC2, accounted for 89.8 % of the total variation, with PC1 explaining 83.8 % of the variation and PC2 explaining 6 % of the variation. As shown in Fig. 4(A), the scoring points for different temperature were evenly distributed in each quadrant of the plot. This result suggests that the volatile composition and the character of the changes resulting from the ARPs decomposition during heating are variable with a U-shaped score curve. Meanwhile, as can be seen from Fig. 4(A), higher temperature scores such as 140 °C, 150 °C, 160 °C, 170 °C, and 180 °C were located in the positive region of PC1, while lower temperature scores like 60 °C, 80 °C, 100 °C, and 120 °C were located in the negative region. Among them, 60 °C and 80 °C points were distributed in the third quadrant, 100 °C and 120 °C points were distributed in the second quadrant, 140 °C and 150 °C points were distributed in the first quadrant, and 160 °C, 170 °C and 180 °C points were distributed in the fourth quadrant. This result suggests that temperature has a large effect on volatile composition of ARPs thermal decomposition. Moreover, the relative content of volatiles in the temperature ranges from 60 °C to 140 °C showed a positive correlation with temperature. Corresponding to the loading plot Fig. 4(B), it can be seen that 2,5-dimethylpyrazine, 3-ethyl-2,5-dimethylpyrazine contributes more to the 140 °C temperature point. 2,5-dimethyl-3-(1-methyl-propyl)-pyrazine and 2,3-dimethyl-5-n-propylpyrazine contributes more to the 150 °C temperature point. While n-ethylpyridine, 5,6-dimethyl-2-benzimidazolinone and 2,3-dimethyl-5-(1-methylpropyl)-pyrazine contributes more to the 180 °C temperature point.

The research demonstrates that temperature and time, as processing conditions, as well as water activity and pH, as intrinsic properties of food systems, significantly influence the extent of the Maillard reaction. Additionally, temperature plays a crucial role in determining the formation of pyrazines (Yu et al., 2021). By comparing our findings with the literatures, it is evident that the composition of pyrazines in the thermal decomposition products of ARPs is fundamentally consistent with previous reports. However, a notable discrepancy is observed in the formation temperature of pyrazine compounds during the ARPs thermal decomposition, which is distinctly lower than that reported in the literature, accompanied by a significantly higher content (Lu et al., 2005; Van Lancker et al., 2010; Van Lancker et al., 2012). This phenomenon can be attributed to the fact that the Amadori rearrangement reaction serves as the rate-limiting step of the entire Maillard reaction (Jalbout et al., 2007). Furthermore, compared to the Maillard reaction substrates reported in the literature, glucose and alanine, as reactants, possess simpler structures, which facilitate the occurrence of the Maillard reaction to a greater extent.

3.4. DFT study on forming mechanism of 3-ethyl-2,5-dimethylpyrazine from ARPs thermal decomposition

The mechanism of 3-ethyl-2,5-dimethylpyrazine formation from the thermal decomposition of ARPs in the alanine-glucose Maillard reaction was investigated by using DFT. As illustrated in Fig. 5(A), a comprehensive analysis yielded a total of 23 distinct reactions and 17 corresponding transition states (TS). Additionally, the potential energy distributions and geometrical conformations of each reactant, transition state, intermediate, and product were meticulously determined. The structures of these transition states are depicted in Fig. 5(B).

At the onset of the reaction, an addition reaction ensues between the carbonyl group of the glucose molecule and the amino group of the alanine molecule, leading to the elimination of one water molecule and the formation of a Schiff base (Spanneberg et al., 2010; Zhao et al., 2017). Subsequently, this intermediate cyclizes to yield an N-substituted aldolylamine, which is transformed into the reactive ARPs 1# via the Amadori rearrangement reaction (Su et al., 2023). This ARPs 1# then undergo thermal decomposition to yield various cleavage products

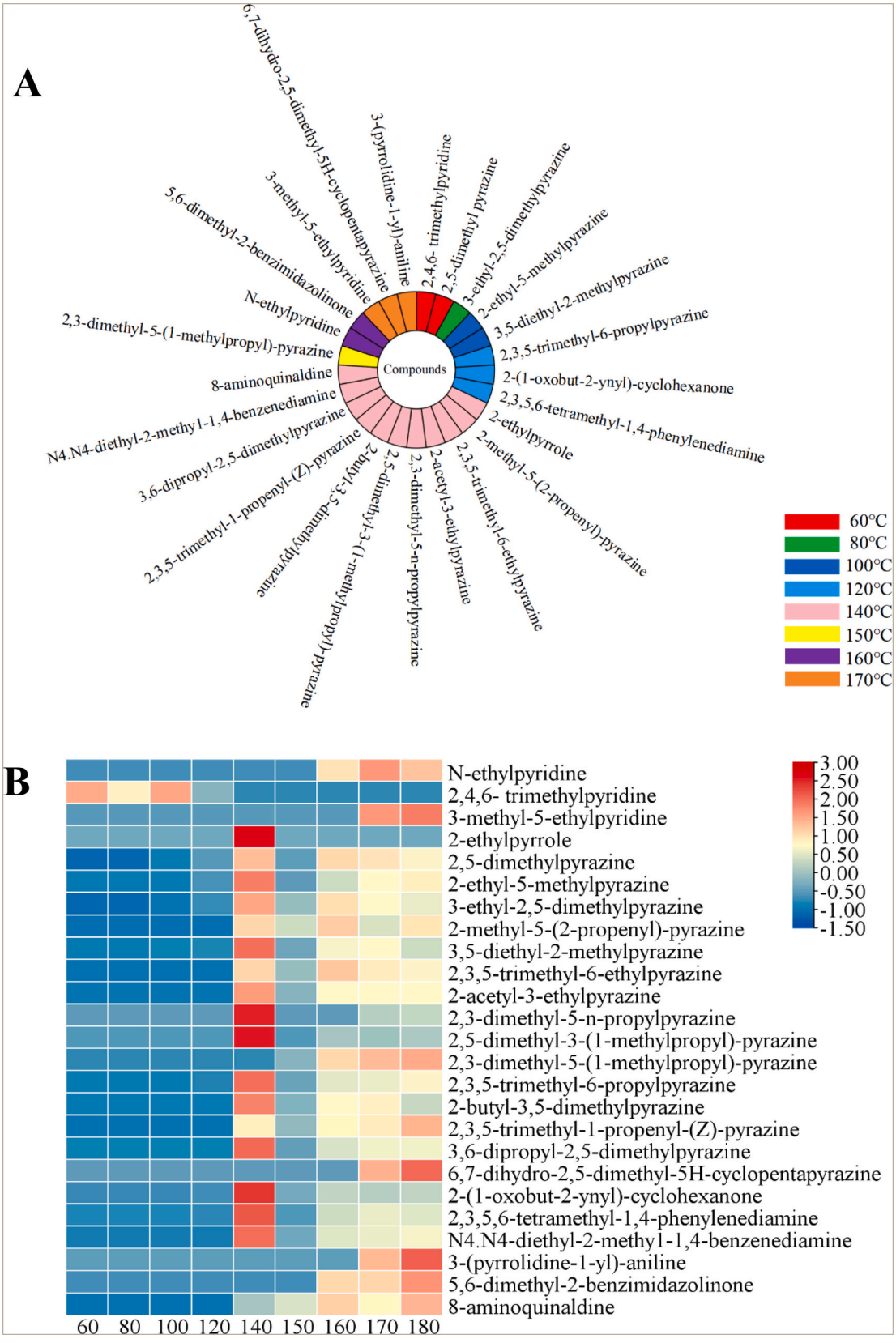

Fig. 3. Results of the temperature effect. A: The forming temperature of different volatile compounds from Alanine - Glucose - ARPs thermal decomposition process. B: Heatmaps of volatile compounds from ARPs decomposition during heating.

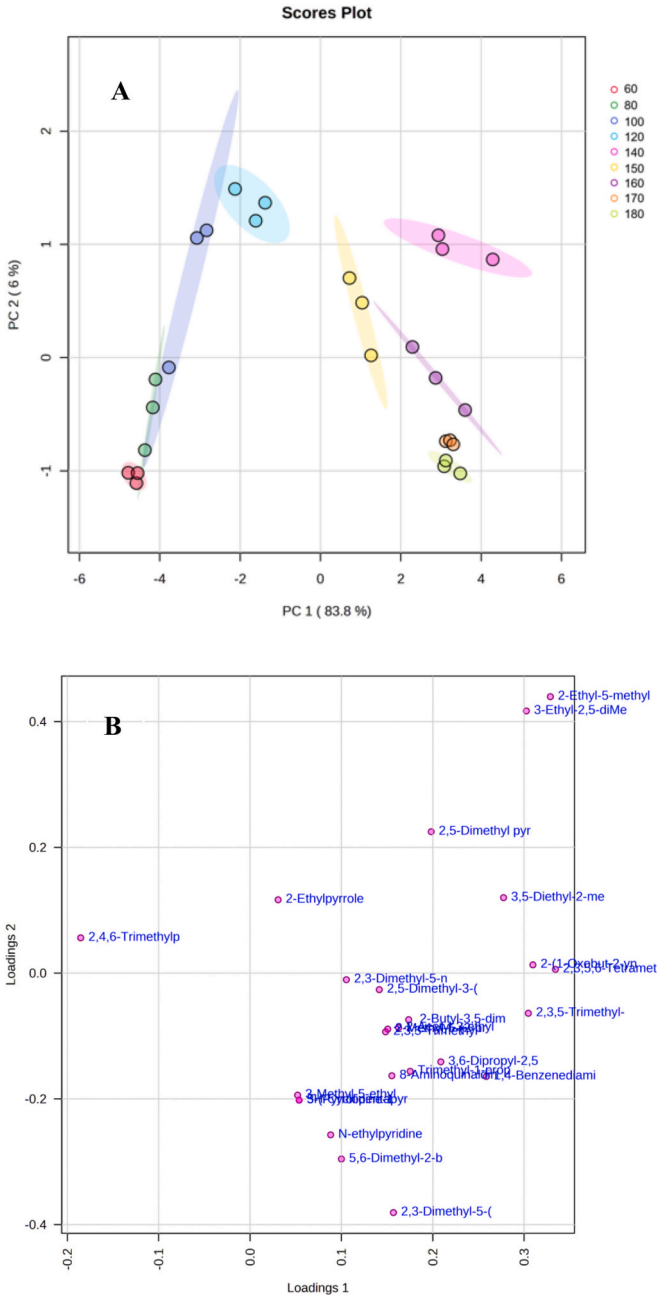

Fig. 4. PCA plots of volatile compounds from Alanine - Glucose - ARPs thermal decomposition process. A: Score scatter plot; B: Loading scatter plot.

under both alkaline and acidic conditions. As depicted in Fig. 5(A), under alkaline conditions, the C1 and C2 positions of ARPs 1# undergo enol isomerization (R1) (Sloop et al., 2006). Specifically, the H atom on C1 attacks the carbon-oxygen double bond, transitioning from the keto form to the enol form with the involvement of transition state TS1#. The energy barrier for this transformation is 249.53 kJ/mol. Subsequently, the rapid loss of an OH^- group from the enol form of the resulting compound 2# generates the Schiff base cation 3# (Shipar, 2004a). Owing to the electron-deficient nature of the N-atom, a nucleophilic addition reaction takes place between OH^- and this N-atom, leading to the formation of compound 4# (Kaya & Kaya, 2015; Shipar, 2006). Compound 4# then loses one molecule of alanine via transition state TS2#, yielding the enol form of 3-deoxyglucosone (R4). The energy barrier for R4 is relatively low at 131.66 kJ/mol (Table S1). Consequently, as illustrated in Fig. 6(B), the rate constant for R4 is significantly higher overall compared to other reactions, indicating that this reaction is more favorable than the others. Following this, 3-deoxyglucosone undergoes enol isomerization (R5) (Wei et al., 2010). Specifically, the transfer of the H atom on the C2 hydroxyl group to C3, via transition state TS3#, results in the conversion of 3-deoxyglucosone from the enol form to the ketone form 6#. The energy barrier for this transformation is 232.32 kJ/mol.

Under acidic conditions, the C2 and C3 positions of ARPs 1# undergo enolic isomerization. Specifically, the H atom on C3 attacks the carbon-oxygen double bond via transition state TS5#, generating compound 7# with a reaction energy barrier of 279.44 kJ/mol. Subsequently, protonation of the molecule (7#) yields the cationic adduct (8#), from which alanine is eliminated to produce the ionic compound 9# (R9) (Southwick & Anderson, 1957). Compound 9# is then deprotonated to form the enol form of 1-deoxyglucosone (10#). Finally, the H atom on the C2 hydroxyl group of compound (10#) transfers to C1 via transition state TS6#, resulting in the keto form of 1-deoxyglucosone (11#). The energy barrier for this transformation is 203.62 kJ/mol.

The decomposition of ARPs represents a pivotal step in the Maillard reaction (Weenen, 1998). Typically, the concentrations of ARP cleavage products are minute; however, their reactivity is pronounced, facilitating the facile formation of more stable products such as glyoxal, acetone aldehyde, and butanedione (Hurt et al., 2013; Zhou et al., 2014). These dicarbonyl compounds are frequently implicated as key intermediates in the synthesis of pyrazines. Furthermore, the degradation of ARPs is predominantly mediated by the reverse aldolization of deoxyglucosone (Shipar, 2004b). Notably, both 1-deoxyketoses and 3-deoxyketoses generate pyruvic aldehydes through retro-aldolization reactions at the C3 and C4 positions of ARPs, respectively. These processes are characterized by transition states, TS4# and TS7#, with corresponding reaction energy barriers of 269.57 kJ/mol and 269.40 kJ/mol.

As depicted in Fig. 5(A), pyruvic aldehyde undergoes a subsequent reaction with alanine in the Strecker reaction, yielding acetaldehyde and carbon dioxide (Kato et al., 2004). The mechanism initiates with the transfer of a hydrogen atom from the nitrogen of alanine to the oxygen of the double bond on the pyruvic aldehyde molecule at the C1 position, thereby forming a hydroxyl group (Vitkovskaya et al., 2017). This is followed by the formation of an addition compound (13#) through the transition state TS8#, with an associated reaction energy barrier of 89.30 kJ/mol. Subsequently, the addition compound (13#) eliminates a molecule of water to generate a Schiff base (14#) via the transition state TS9#, with an energy barrier of 151.26 kJ/mol. The hydrogen atom on the C2 position of the Schiff base (14#) migrates towards the double bond oxygen on the C5 position, adopting an enol configuration (15#) through the transition state TS10#, with a reaction energy barrier of 270.12 kJ/mol. The enol form (15#) then proceeds through a decarboxylation reaction via TS11# to produce compound (16#), with an energy barrier of 192.29 kJ/mol (R16) (Carlsson & Lindqvist, 1962). Compound (16#) undergoes an addition reaction with water molecules at the carbon-ammonia double bond to form compound (17#) via TS12#, with a reaction energy barrier of 91.69 kJ/mol. Compound (17#) is subsequently converted to amino propanone (18#) by the elimination of one molecule of acetaldehyde via TS13#, with an energy barrier of 42.09 kJ/mol. Research has elucidated that Strecker aldehydes serve as crucial flavor substances and significant intermediates in the biosynthesis of numerous other aroma compounds (Turner et al., 2021). Finally, two molecules of amino propanones, in their enol forms, undergo dehydrocyclization to form the unstable 2,5-dimethyl-dihydropyrazine via TS14#, with an energy barrier of 109.37 kJ/mol. This intermediate is further transformed into the stable 3-ethyl-2,5-dimethylpyrazine (23#) through a series of reactions mediated by TS15#-TS17#, with respective energy barriers of −79.17 kJ/mol, 115.67 kJ/mol, and 207.24 kJ/mol.

Fig. 6 (A) illustrates the total potential energy surface for the

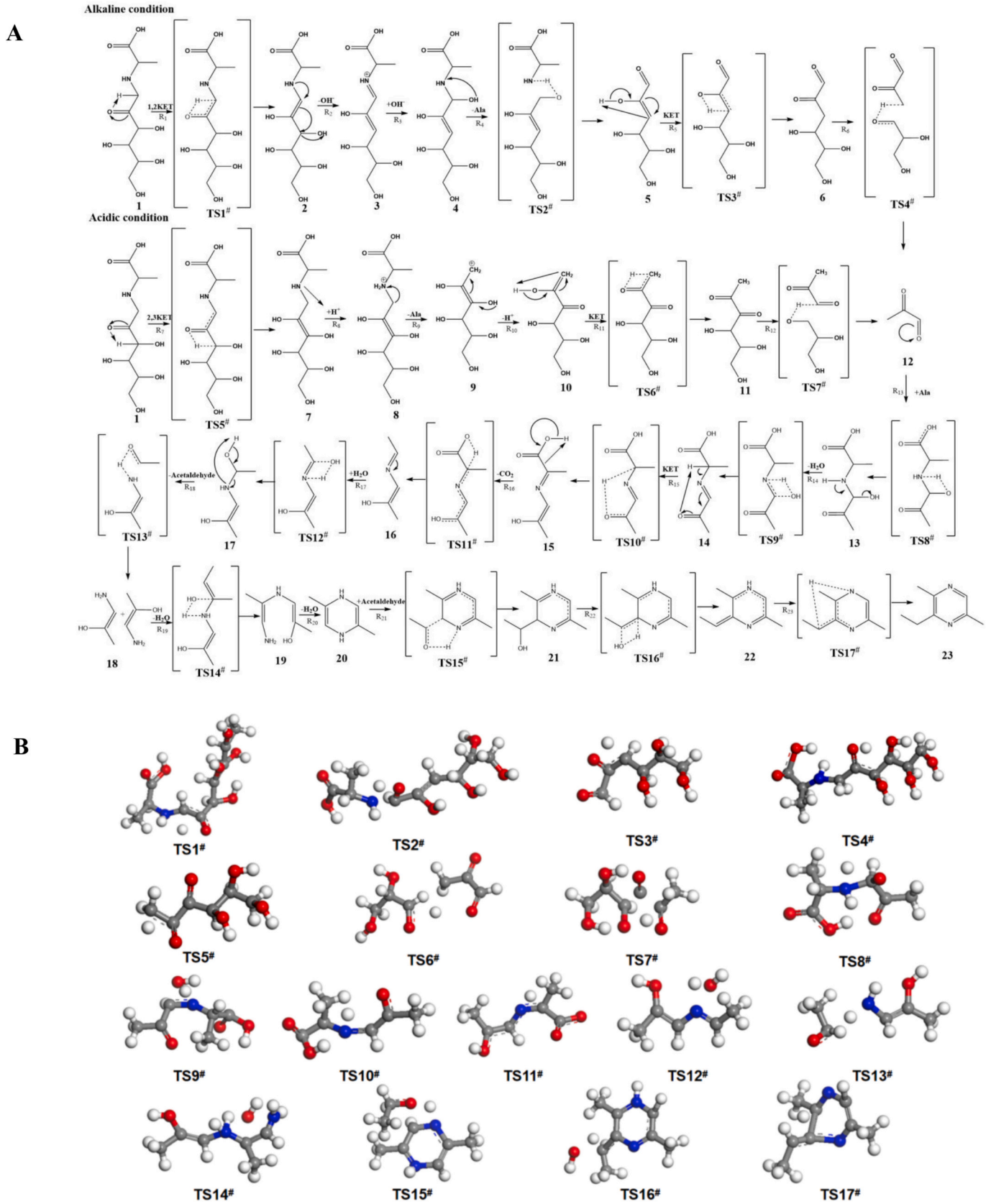

Fig. 5. DFT calculation results. A: Potential forming pathway of 3-ethyl-2,5-dimethylpyrazine during Alanine - Glucose - ARPs thermal decomposition process; B: Transition states involved in the forming pathway of 3-ethyl-2,5-dimethylpyrazine in the ARPs thermal decomposition reaction.

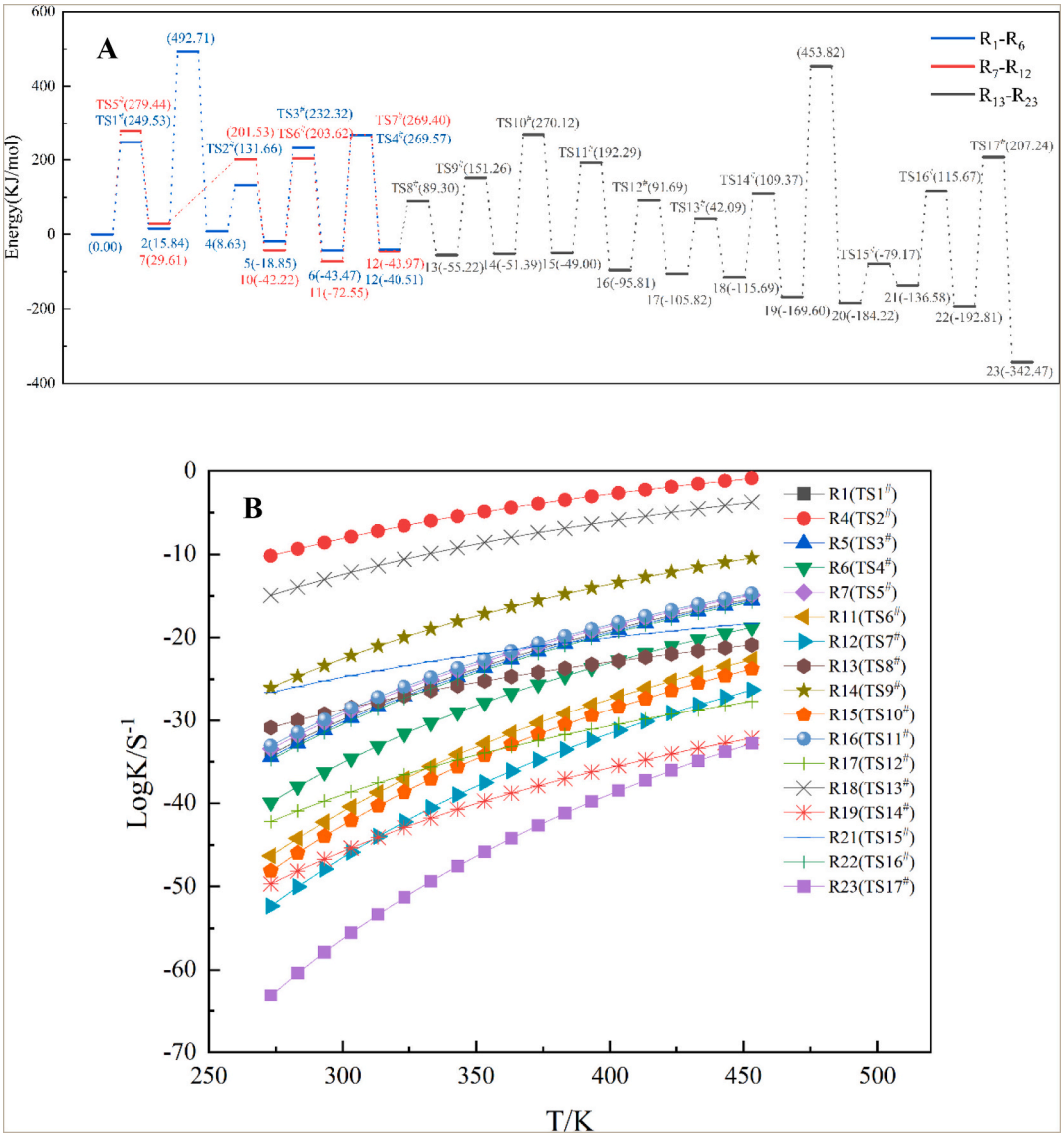

Fig. 6. Potential energy and rate constants of 3-ethyl-2,5-dimethylpyrazine formed in Alanine - Glucose - ARPs thermal decomposition reaction. A: Energy barrier diagram of different reactions; B: Reaction rate constants diagram.

formation of 3-ethyl-2,5-dimethylpyrazine. It reveals that the highest energy barriers for reactions under basic and acidic conditions are 492.71 kJ/mol (R2) and 279.44 kJ/mol (R7), respectively. The energy barriers in the basic pathway are notably higher than those in the acidic pathway, and most of the reaction energy barriers in the basic pathway are generally higher than those under acidic conditions, suggesting that the acidic pathway is more favorable than the basic pathway. Additionally, the ring-closure reaction (R20) of 2,5-dimethyl-dihydropyrazine (20#) is also a reaction with a substantial energy barrier of 453.32 kJ/mol. Consequently, R2, R7, and R20 are identified as critical reactions in the formation pathway of 3-ethyl-2,5-dimethylpyrazine. Furthermore, as depicted in Fig. 6(B), the rate constants of various reactions are profoundly influenced by temperature, with an increase in rate constants as temperature rises. For instance, R23 is a reaction characterized by a relatively high energy barrier and a correspondingly lower reaction rate constant.

4. Conclusions

Pyrazines are the predominant products of the ARPs thermal decomposition derived from the glucose-alanine Maillard reaction, with alkyl pyrazines being particularly abundant. DFT was utilized to investigate the detailed mechanism of 3-ethyl-2,5-dimethylpyrazine formation during the thermal decomposition of ARPs. Results demonstrate that DFT is a powerful tool for analyzing the molecular structures, reaction energy barriers, and reaction rate constants of each reactant, product, intermediate, and transition state involved in the pathway leading to the generation of 3-ethyl-2,5-dimethylpyrazine. Incorporating DFT into the study of Maillard reactions facilitates a comprehensive analysis of the reaction mechanism and the formation of aroma substances. The results indicate that the synthesis of deoxyglucosones can proceed under either acidic or basic conditions, with the acidic pathway being favored over the alkaline pathway. Furthermore, the synthesis of deoxyglucosones and the ring-forming reaction of pyrazines are identified as the critical steps in the overall generation pathway.

CRediT authorship contribution statement

Pengxun Gao: Writing – original draft, Software, Data curation. **Shang Wang:** Writing – review & editing, Methodology. **Baomin Feng:** Writing – review & editing, Resources. **Chunying Liu:** Formal analysis. **Yi Wang:** Software. **Shaohua Dou:** Supervision, Project administration,

Data curation. **Liang Dong:** Supervision, Project administration, Methodology, Funding acquisition.

Declaration of competing interest

The authors declare that they have no known competing financial interests or personal relationships that could have appeared to influence the work reported in this paper.

Acknowledgements

We thank the support of Liaoning Provincial Department of Education University Basic Scientific Research Surface Project (JYTMS20230376); National Natural Science Foundation of China (No. 31871760).

Appendix A. Supplementary data

Supplementary data to this article can be found online at https://doi.org/10.1016/j.fochx.2025.102446.

Data availability

The authors do not have permission to share data.

References

Brittain, J. M., Da La Mare, P. B. D., Isaacs, N. S., & Mclntyre, P. D. (1979). Electrophilic substitution with rearrangement. Part 8. Some products of bromination of 3,4-dimethylphenol; a route to substitution meta- to a hydroxy-group. *Journal of the chemical society, Perkin. Transactions, 2, 7*, 933–937. https://doi.org/10.1039/P29790000933

Cai, L. Y., Li, D. M., Dong, Z. J., Cao, A. L., Lin, H., & Li, J. R. (2016). Change regularity of the characteristics of Maillard reaction products derived from xylose and Chinese shrimp waste hydrolysates. *LWT- Food Science and Technology, 65*, 908–916. https://doi.org/10.1016/j.lwt.2015.09.007

Carlsson, A., & Lindqvist, M. (1962). In-vivo decarboxylation of α-methyl dopa and α-methyl metatyrosine. *Acta Physiologica Scandinavica, 54*(1), 87–94. https://doi.org/10.1111/j.1748-1716.1962.tb02331.x

Cho, S., & Kays, S. J. (2013). Aroma-active compounds of wild rice (zizania palustris l.). *Food Research International, 54*(2), 1463–1470. https://doi.org/10.1016/j.foodres.2013.09.042

Cui, H. P., Yu, J. H., Zhai, Y., Feng, L. H., Chen, P. S., Hayat, K., … Ho, C. T. (2021). Formation and fate of Amadori rearrangement products in Maillard reaction. *Trends in Food Science & Technology, 115*, 391–408. https://doi.org/10.1016/J.tifs.2021.06.055

Evershed, R. P., Morgan, E. D., & Cammaerts, M. C. (1982). 3-ethyl-2,5-dimethylpyrazine, the trail pheromone from the venom gland of eight species of myrmica ants. *Insect Biochemistry, 12*(4), 383–391. https://doi.org/10.1016/0020-1790(82)90035-X

Gaudette, N. J., & Pietrasik, Z. (2017). The sensory impact of salt replacers and flavor enhancer in reduced sodium processed meats is matrix dependent. *Journal of Sensory Studies, 32*(1), Article e12247. https://doi.org/10.1111/joss.12247

Glinsky, G. V., Mossine, V. V., Price, J. E., Bielenberg, D., Glinsky, V. V., Ananthaswamy, H. N., & Milton, S. F. (1996). Inhibition of colony formation in agarose of metastatic human breast carcinoma and melanoma cells by synthetic glycoamine analogs. *Clinical & Experimental Metastasis, 14*, 253–267. https://doi.org/10.1007/BF00053899

Gómez-Míguez, M. J., Cacho, J. F., Ferreira, V., Vicario, I. M., & Heredia, F. J. (2007). Volatile components of Zalema white wines. *Food Chemistry, 100*(4), 1464–1473. https://doi.org/10.1016/j.foodchem.2005.11.045

Guerra, P. V., & Yaylayan, V. A. (2012). Double Schiff base adducts of 2,3-butanedione with glycine: Formation of pyrazine rings with the participation of amino acid carbon atoms. *Journal of Agricultural and Food Chemistry, 60*(45), 11440–11445. https://doi.org/10.1021/jf303658m

Higashio, Y., & Shoji, T. (2004). Heterocyclic compounds such as pyrrole, pyridines, pyrrolidine, piperidine, indole, imidazol and pyrazines. *Applied Catalysis A General, 260*(2), 251–259. https://doi.org/10.1016/S0926-860X(03)00197-2

Hurt, M. R., Degenstein, J. C., Gawecki, P., Borton, D. J., Vinueza, N. R., & Yang, L.N.,… Kenttämaa, H. I.. (2013). On-line mass spectrometric methods for the determination of the primary products of fast pyrolysis of carbohydrates and for their gas-phase manipulation. *Analytical Chemistry, 85*(22), 10927–10934. https://doi.org/10.1021/ac402380h

Jalbout, A. F., Shipar, M. A. H., & Navarro, J. L. (2007). Density functional computational studies on ribose and glycine maillard reaction: Formation of the amadori rearrangement products in aqueous solution. *Food Chemistry, 103*(3), 919–926. https://doi.org/10.1016/j.foodchem.2006.09.045

Kato, N., Suzuki, M., Kanai, M., & Shibasaki, M. (2004). General and practical catalytic enantioselective strecker reaction of ketoimines: Significant improvement through catalyst tuning by protic additives. *Tetrahedron Letters, 45*(15), 3147–3151. https://doi.org/10.1016/j.tetlet.2004.02.082

Kaya, S., & Kaya, C. (2015). A new equation based on ionization energies and electron affinities of atoms for calculating of group electronegativity. *Computational and Theoretical Chemistry, 1052*, 42–46. https://doi.org/10.1016/j.comptc.2014.11.017

Long, R. C., Long, K. R., & Goldstein, J. H. (1973). Orientation and structure of pyrazine, pyrimidine, and pyridazine in a lyotropic liquid crystal. *Molecular Crystals and Liquid Crystals, 21*(3–4), 299–313. https://doi.org/10.1080/15421407308083325

Lu, C. Y., Hao, Z., Payne, R., & Ho, C.T. (2005). Effects of water content on volatile generation and peptide degradation in the Maillard reaction of glycine, diglycine, and triglycine. Journal of Agricultural and Food Chemistry, 53(16), 6443–6447. doi: https://doi.org/10.1021/jf050534p.

Lu, F. S. H., Bruheim, I., Haugsgjerd, B. O., & Jacobsen, C. (2014). Effect of temperature towards lipid oxidation and non-enzymatic browning reactions in krill oil upon storage. *Food Chemistry, 157*, 398–407. https://doi.org/10.1016/j.foodchem.2014.02.059

Ma, Y. J., Wang, X. Y., Zhu, B. W., Du, M., Dong, L., Dong, X. P., & Xu, X. B. (2022). Model studies on the formation of 2-vinylpyrazine and 2-vinyl-6-methylpyrazine in Maillard-type reactions. *Food Chemistry, 374*, 131652. https://doi.org/10.1016/J.FOODCHEM.2021.131652

Mizuguchi, J. (2005). A pigment precursor based on 1,4-diketo-3,6-diphenyi-pyrrolo [3,4-c]-pyrrole and its regeneration into the pigment. *Journal of Imaging Science and Technology, 49*(1), 35–40. https://doi.org/10.2352/J.ImagingSci.Technol.2005.49.1.art00005

Mortzfeld, F. B., Hashem, C., Vranková, K., Winkler, M., & Rudroff, F. (2020). Pyrazines: Synthesis and industrial application of these valuable flavor and fragrance compounds. *Biotechnology Journal, 15*(11), 2000064. https://doi.org/10.1002/biot.202000064

Motoyama, T., Nakano, S., Hasebe, F., Miyata, Y., Kumazawa, S., Miyoshi, N., & Ito, S. (2021). Chemoenzymatic synthesis of 3-ethyl-2,5-dimethylpyrazine by L-threonine 3-dehydrogenase and 2-amino-3-ketobutyrate CoA ligase/L-threonine aldolase. *Communications Chemistry, 4*, 108. https://doi.org/10.1038/s42004-021-00545-8

Nagai, R., Shirakawa, J., Fujiwara, Y., Ohno, R., Moroishi, N., Sakata, N., & Nagai, M. (2014). Detection of AGEs as markers for carbohydrate metabolism and protein denaturation. *Journal of Clinical Biochemistry and Nutrition, 55*(1), 1–6. https://doi.org/10.3164/jcbn.13-112

Orhan, E., Pontes, F. M., Pinheiro, C. D., Longo, E., Pizani, P. S., Varela, V. A., & Andrés, J. (2005). Theoretical and experimental study of the relation between photoluminescence and structural disorder in barium and strontium titanate thin films. *Journal of the European Ceramic Society, 25*(12), 2337–2340. https://doi.org/10.1016/j.jeurceramsoc.2005.03.053

Parr, R. G. (1980). Density-functional theory of atoms and molecules. In K. Fukui, & B. Pullman (Eds.), *Vol. 3. Horizons of quantum chemistry. Académie Internationale des sciences Moléculaires Quantiques/international academy of quantum molecular science*. Dordrecht: Springer. https://doi.org/10.1007/978-94-009-9027-2_2.

Portella, G., Terrazas, M., Villegas, N., González, C., & Orozco, M. (2015). Can a denaturant stabilize DNA? Pyridine reverses DNA denaturation in acidic pH. *Angewandte Chemie, 127*(36), 10634–10637. https://doi.org/10.1002/ange.201503770

Quapp, W. (2010). Finding the transition state without initial guess: The growing string method for newton trajectory to isomerization and enantiomerization reaction of alanine dipeptide and poly(15)alanine. *Journal of Computational Chemistry, 28*(11), 1834–1847. https://doi.org/10.1002/jcc.20688

Shipar, H. A. M. (2004a). Computational studies on glyceraldehyde and glycine Maillard reaction-II. *Journal of Molecular Structure: THEOCHEM, 710*(1–3), 65–71. https://doi.org/10.1016/j.theochem.2004.09.003

Shipar, H. A. M. (2004b). Computational studies on glyceraldehyde and glycine Maillard reaction- III. *Journal of Molecular Structure: THEOCHEM, 712*(1–3), 39–47. https://doi.org/10.1016/j.theochem.2004.09.017

Shipar, H. A. M. (2006). Formation of pyrazines in dihydroxyacetone and glycine Maillard reaction: A computational study. *Food Chemistry, 98*(3), 403–415. https://doi.org/10.1016/j.foodchem.2005.04.023

Sloop, J. C., Bumgardner, C. L., Washington, G., Loehle, W. D., Sankar, S. S., & Lewis, A. B. (2006). Keto–enol and enol–enol tautomerism in trifluoromethyl-β-diketones. *Journal of Fluorine Chemistry, 127*(6), 780–786. https://doi.org/10.1016/j.jfluchem.2006.02.012

Southwick, P. L., & Anderson, J. E. (1957). The stereochemistry of conjugate additions. A study of the addition of amines to (2-nitropropenyl)-benzene. *Journal of the American Chemical Society, 79*(23), 6222–6229. https://doi.org/10.1021/ja01580a031

Spanneberg, R., Osswald, F., Kolesov, I., Anton, W., Radusch, H. J., & Glomb, M. A. (2010). Model studies on chemical and textural modifications in gelatin films by reaction with glyoxal and glycolaldehyde. *Journal of Agricultural and Food Chemistry, 58*(6), 3580–3585. https://doi.org/10.1021/jf9039827

Su, G. W., Yu, Z. X., Wang, H. Y., Zhao, M. M., Zhao, T. T., & Zhang, J. N. (2023). Impact of ternary NADES prepared from proline, glucose and water on the Maillard reaction: Reaction activity, Amadori compound yield, and taste-enhancing ability. *Food Chemistry: X, 20*, Article 100905. https://doi.org/10.1016/J.FOCHX.2023.100905

Takken, H. J., Van Der Linde, L. M., Boelens, M., & Van Dort, J. M. (1975). Olfactive properties of a number of polysubstituted pyrazines. *Journal of Agricultural and Food Chemistry, 23*(4), 638–642. https://doi.org/10.1021/jf60200a053

Tan, Z. W., & Yu, A. N. (2012). Volatiles from the Maillard reaction of l-ascorbic acid with l-glutamic acid/l-aspartic acid at different reaction times and temperatures. *Asia-Pacific Journal of Chemical Engineering, 7*(4), 563–571. https://doi.org/10.1002/apj.607

Turner, L., Lignou, S., Gawthrop, F., & Wagstaff, C. (2021). Investigating the factors that influence the aroma profile of apium graveolens: A review. *Food Chemistry, 345*, Article 128673. https://doi.org/10.1016/j.foodchem.2020.128673

Van Lancker, F., Adams, A., & De Kimpe, N. (2010). Formation of pyrazines in Maillard model systems of lysine-containing dipeptides. *Journal of Agricultural and Food Chemistry, 58*(4), 2470–2478. https://doi.org/10.1021/jf903898t

Van Lancker, F., Adams, A., & De Kimpe, N. (2012). Impact of the *N*-terminal amino acid on the formation of pyrazines from peptides in Maillard model systems. *Journal of Agricultural and Food Chemistry, 60*(18), 4697–4708. https://doi.org/10.1021/jf301315b

Vitkovskaya, N. M., Kobychev, V. B., Bobkov, A. S., Orel, V. B., Schmidt, E. Y., & Trofimov, B. A. (2017). Nucleophilic addition of ketones to acetylenes and allenes: A quantum-chemical insight. *The Journal of Organic Chemistry, 82*(23), 12467–12476. https://doi.org/10.1021/acs.joc.7b02263

Wang, B. C., Wang, S., Wang, Y., Zhang, S. F., Lin, X. P., Xu, X. B., … Dong, L. (2023). Deep exploration of lipid oxidation into flavor compounds: A density functional theory study on (E)-2-decenal thermal oxidative reaction. *Food Chemistry, 428*, 136725. https://doi.org/10.1016/J.FOODCHEM.2023.136725

Weenen, H. (1998). Reactive intermediates and carbohydrate fragmentation in maillard chemistry. *Food Chemistry, 62*(4), 393–401. https://doi.org/10.1016/S0308-8146(98)00074-0

Wei, X. F., Zhang, D. J., Zhang, C. Q., & Liu, C. B. (2010). Theoretical study of the michael addition of acetylacetone to methyl vinyl ketone catalyzed by the ionic liquid 1-butyl-3-methylimidazolium hydroxide. *International Journal of Quantum Chemistry, 110*(5), 1056–1062. https://doi.org/10.1002/qua.22028

Won, D. H., & Lee, C. H. (2001). Thiophene-containing Schiff-base macrocycles: Intermediate compounds between macroaromatics and azamacrocycles. *Tetrahedron Letters, 42*(10), 1969–1972. https://doi.org/10.1016/S0040-4039(01)00093-4

Yu, A. N., Tan, Z. W., & Wang, F. S. (2013). Mechanistic studies on the formation of pyrazines by Maillard reaction between L-ascorbic acid and L-glutamic acid. *LWT-Food Science and Technology, 50*(1), 64–71. https://doi.org/10.1016/j.lwt.2012.07.001

Yu, H., Zhang, R. Y., Yang, F. W., Xie, Y. F., Guo, Y. H., Yao, W. R., & Zhou, W. B. (2021). Control strategies of pyrazines generation from Maillard reaction. *Trends in Food Science & Technology, 112*, 795–807. https://doi.org/10.1016/j.tifs.2021.04.028

Yu, X. H., Cui, H. P., Hayat, K., Hussain, S., Jia, C. S., Zhang, S. L., … Ho, C. T. (2019). Effective mechanism of (−)-epigallocatechin Gallate indicating the critical formation conditions of Amadori compound during an aqueous Maillard reaction. *Journal of Agricultural and Food Chemistry, 67*(12), 3412–3422. https://doi.org/10.1021/acs.jafc.9b00034

Zhao, H. L., Tang, S. S., Xu, X., & Du, L. (2017). Hydrogen bonding interaction between atmospheric gaseous amides and methanol. *International Journal of Molecular Sciences, 18*(1), 4. https://doi.org/10.3390/ijms18010004

Zhou, X. W., Nolte, W. M., Shanks, H. B., & Broadbelt, L. J. (2014). Experimental and mechanistic modeling of fast pyrolysis of neat glucose-based carbohydrates. 2. Validation and evaluation of the mechanistic model. *Industrial & Engineering Chemistry Research, 53*(34), 13290–13301. https://doi.org/10.1021/ie502260q